Journal of Non-Crystalline Solids 447 (2016) 267–272

Contents lists available at ScienceDirect

Journal of Non-Crystalline Solids

journal homepage: www.elsevier.com/locate/jnoncrysol

Elastic moduli of $XAlSiO_4$ aluminosilicate glasses: effects of charge-balancing cations

Coralie Weigel [a], Charles Le Losq [b,c], Rémy Vialla [a], Christelle Dupas [a], Sébastien Clément [a], Daniel R. Neuville [b], Benoit Rufflé [a,*]

[a] Laboratoire Charles Coulomb, UMR-CNRS 5221, Université de Montpellier, F-34095 Montpellier, France
[b] CNRS-IPGP, Géomatériaux, Sorbonne Paris Cité, 1 rue Jussieu, 75005 Paris, France
[c] Research School of Earth Sciences, The Australian National University, Building 142, Mills Road, Canberra ACT 2601, Australia

ARTICLE INFO

Article history:
Received 2 May 2016
Received in revised form 10 June 2016
Accepted 15 June 2016
Available online xxxx

Keywords:
Aluminosilicate glasses
Tectosilicate
Elastic properties
Density
Glass transition temperature
Brillouin scattering

ABSTRACT

Brillouin spectroscopy is used to investigate the elastic properties of $XAlSiO_4$ aluminosilicate glasses where X = Li, Na, K, $Mg_{0.5}$, $Ca_{0.5}$, $Sr_{0.5}$, $Ba_{0.5}$, and $Zn_{0.5}$. The Brillouin frequency shifts obtained in two different scattering geometries allow the calculation of the refractive index, the two sound velocities and Poisson's ratio. Measurements of the mass density give in turn the elastic moduli and the Debye temperature. We find that the elastic properties scale with the atomic density of the glassy network or the charge-balancing cation field strength while they negatively correlate with the glass transition temperature. Further, Poisson's ratio depends on the nature of the non-framework cations in this glass series.

1. Introduction

About 85% of the atoms in the Earth's crust are oxygen and silicon atoms forming a myriad of silicate compounds when combined with alkali, alkaline earth or other metals. Aluminum being the most abundant metal in the crust, the crucial role of aluminosilicates in earth sciences is manifest. High-value aluminosilicate glasses and glass-ceramics are widely used in currently emerging technologies due to their attractive mechanical, optical or refractory properties [1,2].

Elasticity is a fundamental property of materials and as such is used in the determination of various physical properties in glass science, such as thermal shock resistance, thermal optical coefficients or fracture toughness. Indeed, the elastic modulus gives a global view of a material stiffness and reflects both the network connectivity and the inter-atomic potentials. It is then quite surprising to observe that the elastic properties of some simple glass compositions, *e.g.* ternary aluminosilicate glasses, are not known yet. It probably relies on the difficulty of bypassing the crystallization for some compositions, and further, on obtaining sufficiently large bubble-free samples to carry on ultrasonic experiments.

In the present paper, we investigate physical properties of a series of charge-compensated aluminosilicate glasses comprising 50% mol SiO_2. The total concentration of charge compensator oxides being equal to that of alumina, the glass structure is expected to be an almost fully connected, three-dimensional, random aluminosilicate network of tetrahedral units in which the charge compensation for the negatively charged $(AlO_4)^-$ tetrahedra would be provided by the $X^{n+}_{2/n}$ cations [3–5]. Actually, these simple stoichiometric considerations must be revised since five-fold coordinated aluminum species have been shown to exist in such tectosilicate glasses [6–13], their content being related to the X cation field strength [11,13] as well as to the SiO_2 content [10,11]. High temperature data also suggest that five-fold Al concentration increases with increasing temperature in tectosilicate melts [14]. We measured density, glass transition temperature, refractive index and sound velocities from which we calculated molar volume, elastic moduli and Debye temperature. The variation of the measured physical properties in these glasses, which should reflect the influence of the charge compensator cations only, is discussed.

2. Experimental methods

2.1. Glass synthesis

The eight charge-balanced $(X^{n+}_{2/n}O^{2-}/Al_2O_3 = 1)$ aluminosilicate glasses were prepared by melting the appropriate quantities of high-purity oxide and carbonate powders according to the following protocol [15]. About 100 g of batch materials (Rectapur, Merck) was mixed and

* Corresponding author.
E-mail address: benoit.ruffle@univ-montp2.fr (B. Rufflé).

http://dx.doi.org/10.1016/j.jnoncrysol.2016.06.023
0022-3093/

brunched for 60 min in alcohol using an agate mortar. The mixture was slowly heated for 24 and 72 h for alkaline earth- and alkali-bearing compositions, respectively, to decompose the carbonate, and then, heated up to 1900 K in a covered platinum crucible for a few hours in equilibrium with air. The melt was quenched in few seconds by dipping the bottom of the platinum crucible into distilled water, leading to an estimated quenching rate of ≃15 K/mn [11] across the glass transition region. This process was repeated four times to warrant the best glass homogeneity.

Glasses containing SrO and BaO oxides are hardly obtained by the above standard quenching technique due to the high liquidus temperature. Ceramic materials were then first synthesized using five melting and crunching steps [16,10]. Small amounts of materials were finally melted using an aerodynamic levitation device in air located at the CEMHTI-CNRS, Orléans, France and a CO_2 laser as the heating source [17]. The melting time was about 1 min. A high quenching rate of ≃300 K/mn [11] was obtained by simply switching off the power source. Clear glass beads with 1–5 mm in diameter were obtained.

All the glasses investigated here were annealed for at least 12 h at about 50–100 K below the estimated T_g. Chemical homogeneity was checked by microprobe analysis and Raman spectroscopy. The samples are labeled XA50.25 according to the charge balancing oxide $X^{\eta+}_{2/n}O^{2-}$ and to the composition comprising 50% mol SiO_2 and 25% mol Al_2O_3. Mass densities ρ were measured with the Archimedes' method in toluene from which we deduced molar volumes V_m. Glass transition temperatures T_g were determined from viscosity measurements. By definition, T_g corresponds to the temperature at which the viscosity is equal to 10^{12} Pa.s. Viscosity measurements were performed using a creep apparatus as detailed in [15,18,19].

2.2. Brillouin scattering

Brillouin scattering experiments were performed using a standard triple-pass tandem interferometer of the Vernier type designed by JRS Scientific Instruments [20]. A single line diode-pumped solid-state laser operating at $\lambda_0 = 532.03$ nm was used to excite the samples with a power of 150 mW at the sample surface. A single photon counting avalanche photo-diode was used to record the Brillouin spectra which were taken at room temperature in both backscattering and symmetric platelet scattering geometry [21] without any polarization analysis. The backscattered light was collected by a high numerical aperture aspheric lens (NA = 0.38). In the platelet geometry, the scattered light was collected at $\theta = 50^{\circ}$ to the incident laser beam by the same aspheric lens. However, the aperture was limited to a curved slit according the spurious geometrical broadening of the Brillouin lines to the resolution of the spectrometer [22]. All the measurements were performed on samples that were optically polished on two opposite parallel faces.

For isotropic materials in backscattering geometry, sound velocities v are related to the measured Brillouin frequency shifts ν_B by the following equation:

$$v = \frac{\nu_B \lambda_0}{2n}, \tag{1}$$

where λ_0 is the incident laser wavelength in air and n is the refractive index of the sample at λ_0. The measured Brillouin lineshapes were analyzed taking into account the slight downshift of the frequency line arising from the finite aperture [23]. In the symmetric platelet geometry, the Brillouin equation reads:

$$v = \frac{\nu_B \lambda_0}{2\sin(\theta/2)}. \tag{2}$$

Selection rules governing Brillouin scattering in isotropic materials show that longitudinal modes only are visible in perfect backscattering geometry whereas both transverse and longitudinal modes can be measured in the symmetric platelet configuration. With combining measurements in both geometries, it is possible to obtain the two sound velocities v_L, v_T and the refractive index of the sample at λ_0. The value of θ was obtained using the Brillouin scattering from the longitudinal mode of a high purity silica glass sample (Suprasil F300, <1 ppm OH) in both geometries (Eq. (1) and (2)) and its known refractive index $n = 1.4607$ at 532 nm. We found $\theta = 49.80^{\circ} \pm 0.16^{\circ}$.

3. Results

3.1. Thermo-physical properties

Table 1 summarizes the measured values of the glass transition temperature T_g and the mass density ρ, as well as the calculated molar volume V_m of the eight tectosilicate glasses. Alkali containing glasses share an almost constant ρ value with a variation of about 1% around 2.46 g.cm^{-3} whereas the mass density of the alkaline earth glasses increases significantly with the increasing molar weight of the charge compensator oxide, from about 2.68 to 3.30 g.cm^{-3}. Conversely, the atomic density which is inversely proportional to V_m decreases with increasing charge compensator cation size for both the alkali and the alkaline earth glasses. As shown in Fig. 1, V_m decreases non-linearly for increasing cation field strength. The latter is here defined as the ratio of the formal charge z divided by the square of the effective cation radius r [32]. Coordination numbers C.N. and corresponding effective radii r [24] used to calculate the cations field strengths z/r^2 are reported in Table 1 for the eight charge-balancing cations. z/r^2 increases along the series $K^+ < Na^+ < Li^+$ and Ba^{2+} $Sr^{2+} < Ca^{2+} < Mg^{2+}$. Accordingly, the cation field strength of the small transition metal cation Zn^{2+} is close to the one of Mg^{2+}. This trend in V_m probably reflects a tighter binding of oxygens to the lighter charge compensator cations, as expected from their larger field strength.

Fig. 2 displays the glass transition temperature as a function of the cation field strength. T_g decreases with z/r^2, both for alkali and alkaline earth glasses, but with very different slopes. For alkali-bearing or alkaline earth-bearing glasses, T_g is thus strongly influenced by the radius of the charge compensator cation. These trends are mostly in line with the viscosity of silica-richer $XAlSi_3O_8$ melts close to T_g which increases in the order Li < Na < Ca < Mg < K [33]. We note however that for the $XAlSiO_4$ glasses here investigated, the T_g of the Ca-bearing glass is higher than the T_g of the Mg compound, in agreement with the smaller radius of the later cation. Such remarkable variations of T_g reveal a strong coupling between the aluminosilicate backbone and the non-framework cation introduced to charge-balance Al in tetrahedral coordination. It has indeed been shown that increasing the field strength of charge compensator cations leads to increasing perturbations and weakening of the aluminosilicate framework [34]. While the trends observed independently for the alkali- or alkaline earth-bearing glasses follow this simple scenario, the substitution of alkaline earth for alkali cations cannot be reconciled with it. The T_g variations could also result from modifications of the aluminosilicate network topology and/or differences in (Si, Al) distributions between alkali- and alkaline earth-bearing glasses [33,35].

3.2. Elastic properties

Fig. 3 shows the Brillouin scattering spectrum from the calcium-bearing aluminosilicate glass obtained in the platelet scattering geometry. For all glasses, both transverse acoustic (TA) and longitudinal acoustic (LA) Brillouin doublets were clearly observed with significant variations of their relative scattered intensities. The intense central unshifted peak is the Rayleigh line, whereas the outer pair of peaks arises from the Rayleigh ghosts of the first order transmitted by the tandem interferometer.

Poisson's ratio v can be readily obtained from the measured Brillouin frequency shifts of the longitudinal ν_{B_L} and the transverse ν_{B_T} modes in

Table 1
Glass label, charge compensator oxide, density ρ, molar volume V_m, cation coordination number C.N., cation effective ionic radius r, cation field strength z/r^2, atomic packing factor C_g and glass transition temperature T_g for the eight tectosilicate glasses under study.

Glass ID	$X^{n+}_{2/n}O^{2-}$	ρ g.cm^{-3}	V_m cm^3.mol^{-1}	C.N.	r Å	z/r^2 Å^{-2}	C_g	T_g K
LA50.25	Li_2O	2.431	25.91	6 [24]	0.82	1.49	0.481	922 [25]
NA50.25	Na_2O	2.494	28.48	7 [26]	1.20	0.69	0.490	1074
KA50.25	K_2O	2.463	32.11	9 [27]	1.60	0.39	0.528	1193
MA50.25	MgO	2.678	24.50	6 [28]	0.80	3.12	0.494	1082
CA50.25	CaO	2.690	25.85	7–8 [26,29]	1.15	1.51	0.493	1131
SA50.25	SrO	3.021	26.95	8 [30]	1.33	1.13	0.492	1152
BA50.25	BaO	3.300	28.44	8 [30]	1.50	0.89	0.489	1149 [31]
ZA50.25	ZnO	3.091	24.55	6 [24]	0.80	3.12	0.493	1022

this geometry with an accuracy of ±0.6%, *i.e.* down to the third digit:

$$\nu = \frac{1}{2}\frac{\left(v_{B_L}^2 - 2v_{B_T}^2\right)}{\left(v_{B_L}^2 - v_{B_T}^2\right)} \tag{3}$$

The hypersonic velocities v_L and v_T were computed from the measured Brillouin shifts and the known external scattering angle θ using Eq. (2), see Table 2. Uncertainty is approximately ±0.5%, mostly arising from the initial determination of θ.

Transverse modes can be actually detected in backscattering Brillouin experiments on isotropic materials using high-NA collection optics. For a near backscattering angle θ', intensity of the TA modes is indeed proportional to $\sin^2\alpha/2$ where $\alpha = \pi - \theta'$. A high-NA backscattering spectrum obtained on the calcium aluminosilicate glass is shown in Fig. 4. Beside the intense LA modes, a clear signature of the TA excitations is observed with an intensity comparable to that obtained using the symmetric platelet scattering geometry. It is a very convenient way to measure Poisson's ratio for samples that cannot be easily prepared as transparent platelets. We report in Table 2 Poisson's ratio ν_{bs} derived from the backscattering data together with those derived from the platelet geometry, showing a very good agreement. Accuracy of ν_{bs} is about ±1%.

Sound velocity data were further combined with sample density to calculate the elastic constants using the following relations, written in such a way that uncertainty calculation can be easily carried out:

$$M = C_{11} = \rho v_L^2 \tag{4}$$

$$G = C_{44} = \rho v_T^2 \tag{5}$$

$$B = \frac{M}{3}\frac{1+\nu}{1-\nu} \tag{6}$$

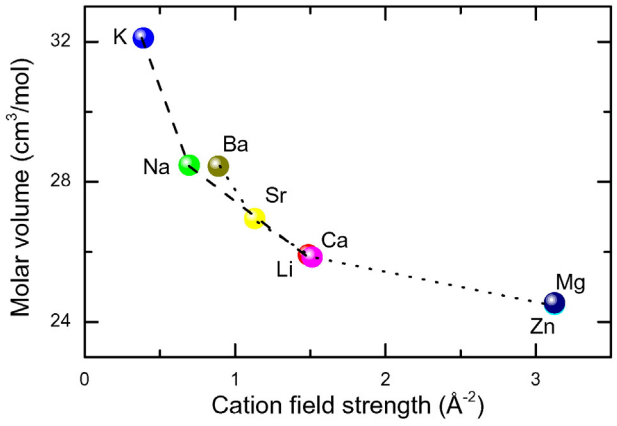

Fig. 1. Molar volume V_m as a function of the cation field strength z/r^2. Plotted values are labeled with the charge balancing cations. Dashed and dotted lines, linking alkali- and alkaline earth-containing glasses respectively, are guides for the eye.

$$E = 2G(1+\nu) \tag{7}$$

The longitudinal M, shear G, bulk B, and Young's E moduli are reported in Table 2. The overall uncertainty of the derived elastic moduli is approximately ±1%. The elastic moduli compare very well with literature data for the Na [36,37] and Ca [38,39] bearing glasses whereas significant different values can be found for the Li containing glass [40]. The much lower mass density of the sample investigated in the later work, $\rho = 2.363$ g.cm^{-3}, as compared to our value $\rho = 2.431$ g.cm^{-3} that agrees with recent work [25], indicates that the data reported in [40] for LA50.25 likely refers to a glass with a slightly different composition.

The Debye temperature θ_D can be derived from the sound velocities as well, following the standard relation:

$$\theta_D = \frac{h}{k_b}\left(\frac{9\mathcal{N}}{4\pi V_a}\right)^{1/3}\left[\frac{1}{v_L^3} + \frac{2}{v_T^3}\right]^{-1/3} \tag{8}$$

where h is the Planck's constant, k_b the Boltzmann's constant, $\mathcal{N}$ the Avogadro's number, and V_a the atomic volume. The Debye temperature represents the temperature at which all vibrational modes are excited, and allows to estimate the vibrational entropy of the glass. As seen in Table 2, θ_D increases with decreasing V_m, alkali-bearing glasses having higher Debye temperatures than alkaline earth ones. From magnesium to barium, a decrease of nearly 150 K, *i.e.* >30%, is observed whereas the difference amounts to 100 K between lithium and potassium.

Finally, the Brillouin frequency shifts of the longitudinal modes obtained in platelet and backscattering geometries were used to estimate the refractive index n at 532 nm using Eqs. (1) and (2). The refractive index, see Table 2, roughly scales with the glass density and increases from about 1.53 for Na and K containing glasses up to about 1.62 for the barium bearing glass. The refractive index is indeed mainly governed by the mean polarisability of the ions forming the glass which generally increases with their number of electrons, *i.e.* a quantity

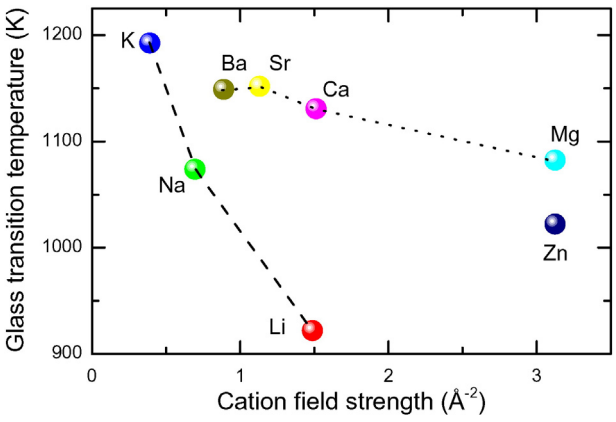

Fig. 2. Glass transition temperature T_g as a function of the charge balancing cation field strength z/r^2.

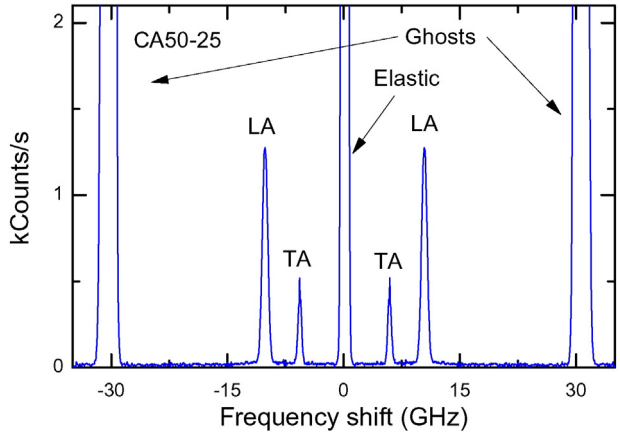

Fig. 3. Typical Brillouin scattering spectrum obtained on the calcium bearing glass in the 50° symmetric platelet geometry. LA(TA) indicate the longitudinal(transverse) modes. The central peak is the elastic scattered intensity, *i.e.* the Rayleigh line, whereas the outer pair of peaks arises from the Rayleigh ghosts of the first order. The spectrum was recorded in about 4 min at room temperature.

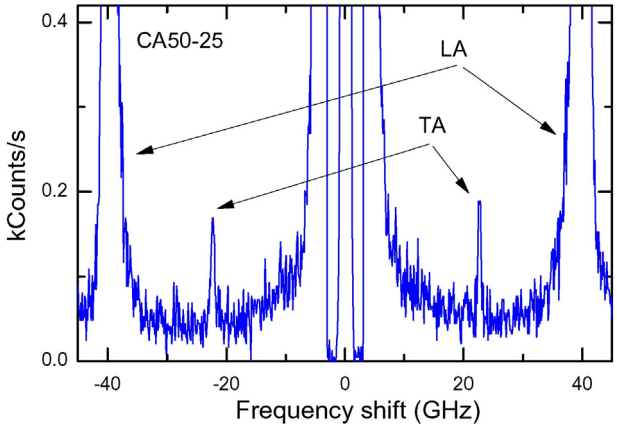

Fig. 4. Typical Brillouin scattering spectrum obtained on the calcium bearing glass in backscattering geometry using high NA optics, showing both longitudinal acoustic (LA) and transverse acoustic (TA) modes. The spectrum was recorded in about 4 min at room temperature.

that is directly related to the atomic mass. It is thus expected to find a good correlation between the refractive index and the glass density and not the molar volume.

4. Discussion

The macroscopic elastic moduli of structural glasses are generally controlled by both the atomic density and the inter-atomic forces. As minor changes of the overall bond energies are foreseen in the investigated glass series, it is expected that atomic density governs the macroscopic elastic properties. This is illustrated in Fig. 5a–c showing the obtained elastic moduli as a function of the molar volume. Shear, bulk and Young's moduli indeed increase with increasing atomic density, *i.e.* with decreasing molar volume. More precisely, alkaline earth aluminosilicate glasses have slightly higher moduli than their alkali counterparts at constant molar volume, a trend which depends on the elastic modulus. While it is hardly visible for the shear modulus, it is clearly seen for the Young's modulus and becomes significant for the bulk modulus. Further, we note that the Zn-bearing glass has the highest elastic moduli of the series and follows identical trends. Finally we observe that the elastic modulus increases with increasing cation field strength as can be inferred from Figs. 1 and 5.

Conversely, an almost constant Poisson's ratio $\nu \simeq 0.234$ is obtained for the three alkali containing glasses (Fig. 6), the sodium bearing glass having the lowest value. The four alkaline earth glasses also display similar Poisson's ratio, albeit slightly higher ones, $\nu \simeq 0.265$. Besides, the zinc containing aluminosilicate glass shows the highest Poisson's ratio $\nu \simeq 0.280$. Whereas the magnitude of the elastic moduli is essentially governed by the atomic density in this series of tectosilicate glasses, it appears that Poisson's ratio is not. Actually, it is often assumed that Poisson's ratio is more closely connected to the glass network connectivity governing the atomic packing factor C_g than to the atomic density or molar volume [41]. C_g is the ratio between the minimum theoretical volume occupied by the ions and the corresponding effective volume of the glass:

$$C_g = \frac{1}{V_m}\sum_i V_i x_i \tag{9}$$

where

$$V_i = \frac{4}{3}\pi\mathcal{N}\left(x r_A^3 + y r_O^3\right) \tag{10}$$

is the molar volume of the ith constituent oxide of molar fraction x_i with A_xO_y chemical formula. In Eq. (10), r_A and r_O are the effective ionic radii taken from [24] for O, Si, and Al whereas $\mathcal{N}$ is the Avogadro number. For the charge compensator cations we used the r values previously mentioned to calculate the cation field strength z/r^2. C_g values are reported in Table 1.

Even if the increase of ν with C_g does not follow a one to one relationship as illustrated in Fig. 7, a faint trend is observed. The modest increase of the Poisson's ratio when going from alkali to alkaline earth-bearing glasses might suggest a progressive decrease of the network dimensionality according to [41]. Recent NMR experiments [13] have indeed shown that the content of "non-stoichiometric" non-bridging oxygen, which amounts to a few percent in $XAlSiO_4$ glasses, is governed by the charge of the cation and not its field strength as opposed to the content of VAl [42]. Alternatively, the increasing Poisson's ratio could reflect modifications of the glassy network topology. Such differences between alkali- and alkaline earth-bearing $XAlSiO_4$ tectosilicate glasses have

Table 2
Longitudinal sound velocity v_L, transverse sound velocity v_T, longitudinal modulus M, shear modulus G, bulk modulus B, Young's modulus E, Poisson's ratio ν, Poisson's ratio ν_{bs} from backscattering data, Debye temperature θ_D, and refractive index n at $\lambda = 532$ nm for the aluminosilicate glasses under study. Numbers in parentheses give uncertainty of the last digit.

Glass ID	v_L km.s$_{-1}$	v_T km.s^{-1}	M GPa	G GPa	B GPa	E GPa	ν	ν_{bs}	θ_D K	n
LA50.25	6.55(3)	3.85(2)	104.3(1.0)	35.9(4)	56.4(7)	88.9(1.1)	0.237(2)	0.241(1)	550(3)	1.564(5)
NA50.25	5.85(3)	3.47(2)	85.4(0.8)	30.1(3)	45.2(6)	73.9(0.8)	0.228(2)	0.228(1)	481(2)	1.533(5)
KA50.25	5.82(3)	3.42(2)	83.4(0.8)	28.8(3)	45.0(6)	71.2(0.8)	0.236(2)	0.234(1)	455(2)	1.532(5)
MA50.25	6.98(3)	3.94(2)	130.6(1.3)	41.5(4)	75.2(9)	105.2(1.2)	0.267(1)	0.270(1)	561(3)	1.585(5)
CA50.25	6.54(3)	3.69(2)	115.0(1.1)	36.5(4)	66.3(8)	92.6(1.1)	0.267(1)	0.267(1)	516(3)	1.604(5)
SA50.25	5.90(3)	3.34(2)	105.0(1.0)	33.8(4)	59.9(7)	85.3(1.0)	0.263(1)	0.265(1)	462(2)	1.596(5)
BA50.25	5.37(3)	3.04(2)	95.1(0.9)	30.6(4)	54.4(8)	77.2(1.2)	0.263(3)	0.262(1)	413(3)	1.619(7)
ZA50.25	6.62(3)	3.66(2)	135.5(1.3)	41.4(4)	80.3(9)	106.1(1.2)	0.280(1)	0.282(1)	523(3)	1.603(5)

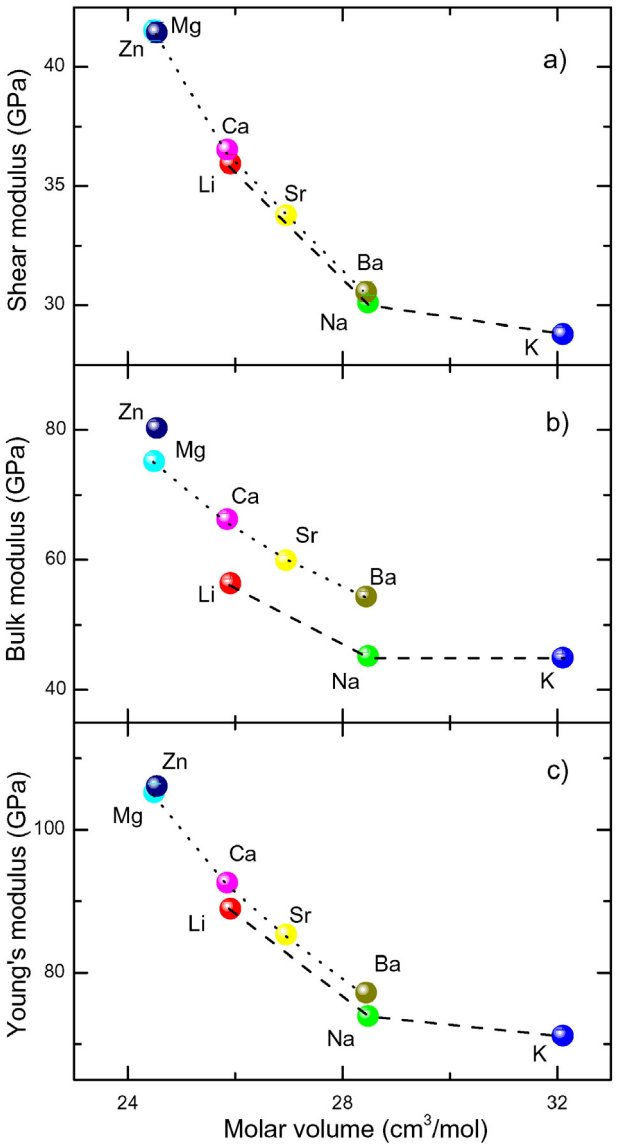

Fig. 5. Elastic moduli of the investigated aluminosilicate glasses as a function of the molar volume V_m: a) shear modulus G, b) bulk modulus B, and c) Young's modulus E.

been evidenced using X-ray diffraction: $NaAlSiO_4$ glass seems mostly formed with six-membered rings containing interstitial alkali cations [4,43,44]. Substitute the alkaline earth cations for alkali ones induces

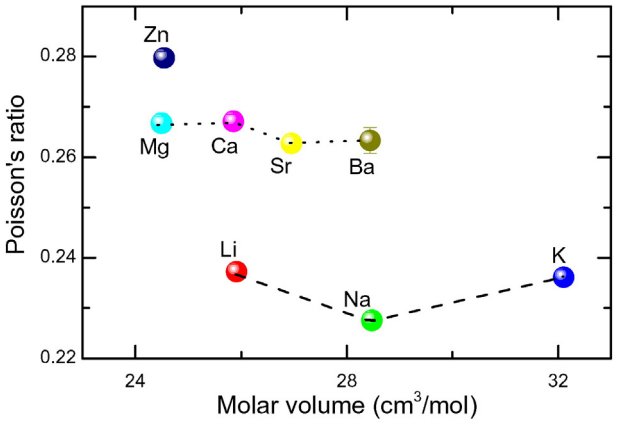

Fig. 6. Poisson's ratio v as a function of the molar volume.

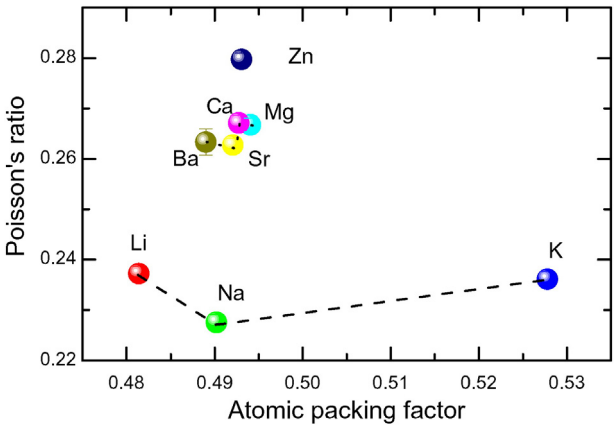

Fig. 7. Poisson's ratio v as a function of the atomic packing factor.

rearrangements of the aluminosilicate framework to maintain local charge balance, *i.e.* two aluminate tetrahedra must be close to each alkaline earth cation, thus leading to a rather different local structure containing more four-membered rings $Al_2Si_2O_8^{2-}$ as in the $Ca_{0.5}AlSiO_4$ case [4,43,44].

However, a striking difference between alkali- and alkaline earth-containing $XAlSiO_4$ glasses is certainly the relation between the cation size and the compactness of the network. While the four alkaline earth-bearing glasses share very similar C_g values in reverse oder of V_m and cation size r, the three alkali glasses show a large increase of C_g *with increasing* V_m and r. In particular, the K bearing glass displays a much higher atomic packing factor, as well as a higher molar volume, as compared to the Na glass implying a marked change in the underlying glass network topology [35].

For chemically closely related glasses, glass transition temperature is often believed to scale with elastic moduli [45]. Striking correlations between Young's modulus and T_g has been reported for example in bulk metallic glasses [46]. On the other hand, glasses formed from completely different chemical species but sharing similar stiffness can span a large range of T_g. We report in Fig. 8 the variation of E with T_g for the investigated glasses, revealing oppositely a negative correlation: T_g increases with decreasing E both for alkali- and alkaline earth-bearing glasses.

5. Conclusion

Charge compensated aluminosilicate glasses with the molar composition $XAlSiO_4$ where X = Li, Na, K, $Mg_{0.5}$, $Ca_{0.5}$, $Sr_{0.5}$, $Ba_{0.5}$, and $Zn_{0.5}$ were synthesized, characterized and investigated using Brillouin light

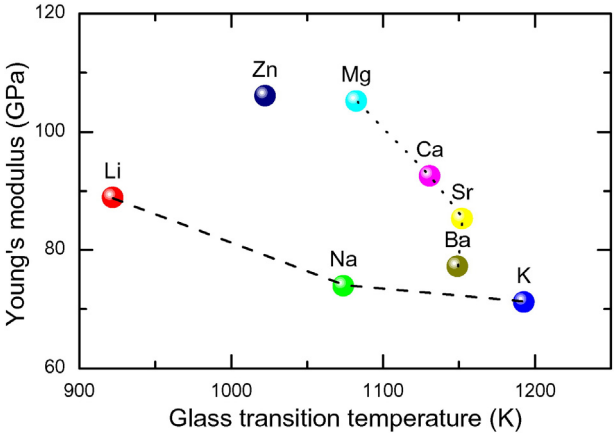

Fig. 8. Young's modulus *versus* glass transition temperature T_g.

scattering. We observe a concomitantly increase of atomic density and elastic moduli with increasing charge-balancing cation field strengths. It likely originates from a tighter binding of the Al-connected oxygen atoms to the lighter cations. Differently, the Poisson's ratio depends on the nature of the charge balancing cations, whether it is an alkali, an alkaline earth or a transition metal, revealing subtle changes in the topology of the aluminosilicate framework. Finally, we also report the negative correlation between the Young's modulus and the glass transition temperature in this glass series.

References

[1] M.E. Lines, J.B. Macchesney, K.B. Lyons, A.J. Bruce, A.E. Miller, K. Nassau, Calcium aluminate glasses as potential ultralow-loss optical-materials at 1.5-1.9 μm, J. Non-Cryst. Solids 107 (2–3) (1989) 251–260.

[2] F.T. Wallenberger, S.D. Brown, High-modulus glass-fibers for new transportation and infrastructure composites and new infrared uses, Compos. Sci. Technol. 51 (2) (1994) 243–263.

[3] B.O. Mysen, D. Virgo, I. Kushiro, The structural role of aluminum in silicate melts - a Raman-spectroscopic study at 1-atmosphere, Am. Mineral. 66 (7–8) (1981) 678–701.

[4] F. Seifert, B.O. Mysen, D. Virgo, 3-dimensional network structure of quenched melts (glass) in the systems SiO_2–$NaAlO_2$, SiO_2–$CaAl_2O_4$ and SiO_2–$MgAl_2O_4$, Am. Mineral. 67 (7–8) (1982) 696–717.

[5] B.O. Mysen, D. Virgo, F.A. Seifert, Relationships between properties and structure of aluminosilicate melts, Am. Mineral. 70 (1–2) (1985) 88–105.

[6] J.F. Stebbins, Z. Xu, NMR evidence for excess non-bridging oxygen in an aluminosilicate glass, Nature 390 (6655) (1997) 60–62.

[7] J.F. Stebbins, S. Kroeker, S.K. Lee, T.J. Kiczenski, Quantification of five- and six-coordinated aluminum ions in aluminosilicate and fluoride-containing glasses by high-field, high-resolution Al-27 NMR, J. Non-Cryst. Solids 275 (1–2) (2000) 1–6.

[8] M.J. Toplis, S.C. Kohn, M.E. Smith, I.J.F. Poplett, Fivefold-coordinated aluminum in tectosilicate glasses observed by triple quantum MAS NMR, Am. Mineral. 85 (10) (2000) 1556–1560.

[9] D.R. Neuville, L. Cormier, D. Massiot, Al environment in tectosilicate and peraluminous glasses: A Al-27 MQ-MAS NMR, Raman, and XANES investigation, Geochim. Cosmochim. Acta 68 (24) (2004) 5071–5079.

[10] D.R. Neuville, L. Cormier, D. Massiot, Al coordination and speciation in calcium aluminosilicate glasses: effects of composition determined by Al-27 MQ-MAS NMR and Raman spectroscopy, Chem. Geol. 229 (1–3) (2006) 173–185.

[11] D.R. Neuville, L. Cormier, V. Montouillout, P. Florian, F. Millot, J.-C. Rifflet, D. Massiot, Structure of Mg- and Mg/Ca aluminosilicate glasses: Al-27 NMR and Raman spectroscopy investigations, Am. Mineral. 93 (11−12) (2008) 1721–1731.

[12] L.M. Thompson, J.F. Stebbins, Non-bridging oxygen and high-coordinated aluminum in metaluminous and peraluminous calcium and potassium aluminosilicate glasses: high-resolution O^{17} and Al^{27} MAS NMR results, Am. Mineral. 96 (5–6) (2011) 841–853.

[13] L.M. Thompson, J.F. Stebbins, Non-stoichiometric non-bridging oxygens and five-coordinated aluminum in alkaline earth aluminosilicate glasses: effect of modifier cation size, J. Non-Cryst. Solids 358 (15) (2012) 1783–1789.

[14] C. Le Losq, D.R. Neuville, P. Florian, G.S. Henderson, D. Massiot, The role of Al^{3+} on rheology and structural changes in sodium silicate and aluminosilicate glasses and melts, Geochim. Cosmochim. Acta 126 (2014) 495–517.

[15] D.R. Neuville, Viscosity, structure and mixing in (Ca, Na) silicate melts, Chem. Geol. 229 (1–3) (2006) 28–41.

[16] D.R. Neuville, L. Cormier, D. De Ligny, J. Roux, A.M. Flank, P. Lagarde, Environments around Al, Si, and Ca in aluminate and aluminosilicate melts by X-ray absorption spectroscopy at high temperature, Am. Mineral. 93 (1) (2008) 228–234.

[17] B. Coté, D. Massiot, F. Taulelle, J.-P. Coutures, ^{27}Al NMR spectroscopy of aluminosilicate melts and glasses, Chem. Geol. 96 (3) (1992) 367–370.

[18] D.R. Neuville, P. Richet, Viscosity and mixing in molten (Ca, Mg) pyroxenes and garnets, Geochim. Cosmochim. Acta 55 (4) (1991) 1011–1019.

[19] D.R. Neuville, Etudes Des Propriétés Thermodynamiques et Rhéologiques Des Silicates Fondus(Ph.D. thesis) Université Paris VII, 1992.

[20] S.M. Lindsay, M.W. Anderson, J.R. Sandercock, Construction and alignment of a high performance multipass Vernier tandem Fabry–Perot interferometer, Rev. Sci. Instrum. 52 (1981) 1478–1486.

[21] C. Weigel, A. Polian, M. Kint, B. Rufflé, M. Foret, R. Vacher, Vitreous silica distends in helium gas: acoustic versus static compressibilities, Phys. Rev. Lett. 109 (2012) 245504.

[22] R. Vialla, B. Rufflé, G. Guimbretière, R. Vacher, Eliminating the broadening by finite aperture in Brillouin spectroscopy, Rev. Sci. Instrum. 82 (11) (2011) 113110.

[23] R. Vacher, S. Ayrinhac, M. Foret, B. Rufflé, E. Courtens, Finite size effects in Brillouin scattering from silica glass, Phys. Rev. B 74 (1) (2006) 012203.

[24] E. Whittaker, R. Muntus, Ionic radii for use in geochemistry, Geochim. Cosmochim. Acta 34 (9) (1970) 945–956.

[25] S. Ross, A.-M. Welsch, H. Behrens, Lithium conductivity in glasses of the Li_2O–Al_2O_3–SiO_2 system, Phys. Chem. Chem. Phys. 17 (2015) 465–474.

[26] D.R. Neuville, L. Cormier, A.M. Flank, V. Briois, D. Massiot, Al speciation and Ca environment in calcium aluminosilicate glasses and crystals by Al and Ca K-edge X-ray absorption spectroscopy, Chem. Geol. 213 (1–3) (2004) 153–163.

[27] L. Losq, Amorphous materials: properties, structure, and durability determination of water content in silicate glasses using raman spectrometry: implications for the study of explosive volcanism, Am. Mineral. 97 (5–6) (2012) 779–790 (le Losq, Charles/0000-0001-8941-9411).

[28] P. Fiske, J. Stebbins, The structural of Mg in silicate liquids - a high-temperature ^{25}Mg, ^{23} Na, and ^{29} Si NMR-study, Am. Mineral. 79 (9–10) (1994) 848–861.

[29] M.R. Cicconi, D. de Ligny, T.M. Gallo, D.R. Neuville, Ca neighbors from XANES spectroscopy: a tool to investigate structure, redox, and nucleation processes in silicate glasses, melts, and crystals, Am. Mineral. 101 (5) (2016) 1232–1235.

[30] A. Novikov, D.R. Neuville, L. Hennet, Y. Gueguen, D. Thiaudière, T. Charpentier, P. Florian, Al and Sr Environment in Tectosilicate Glasses and Melts: Viscosity, Raman and NMR Investigation, 2016 (submitted for publication).

[31] B. Hoghooghi, J. McKittrick, E. Helsel, O.A. Lopez, Microstructural development, densification, and hot pressing of celsian ceramics from ion-exchanged zeolite precursors, J. Am. Ceram. Soc. 81 (4) (1998) 845–852.

[32] A. Dietzel, Die kationenfeldstärken und ihre beziehungen zu entglasungsvorgängen, zur verbindungsbildung und zu den schmelzpunkten von silicaten, Z. Elektrochem. 48 (1) (1949) (9–2).

[33] C. Romano, B. Poe, V. Mincione, K.U. Hess, D.B. Dingwell, The viscosities of dry and hydrous $XAlSi_3O_8$ (X = Li, Na, K, $Ca_{0.5}$, $Mg_{0.5}$) melts, Chem. Geol. 174 (1–3) (2001) 115–132.

[34] A. Navrotsky, K. Geisinger, P. McMillan, G. Gibbs, The tetrahedral framework in glasses and melts — inferences from molecular orbital calculations and implications for structure, thermodynamics, and physical properties, Phys. Chem. Miner. 11 (6) (1985) 284–298.

[35] C. Le Losq, D.R. Neuville, Effect of the Na/K mixing on the structure and the rheology of tectosilicate silica-rich melts, Chem. Geol. 346 (2013) 57–71.

[36] V.Y. Livshits, D.G. Tennison, G.O. Karapetyan, Acoustic and elastic properties of glasses in the Na_2O–Al_2O_3–SiO_2 system, Sov. J. Glas. Phys. Chem. 8 (1982) 285.

[37] V.Y. Livshits, D.G. Tennison, S.B. Gukasyan, A.K. Kostanyan, Acoustic and elastic properties of glasses in the system Na_2O–Al_2O_3 -–SiO_2, Sov. J. Glas. Phys. Chem. 8 (1982) 463.

[38] V. Askarpour, M.H. Manghnani, P. Richet, Elastic properties of diopside, anorthite, and grossular glasses and liquids - a Brillouin-scattering study up to 1400 K, J. Geophys. Res. Solid Earth 98 (B10) (1993) 17683–17689.

[39] A. Pönitzsch, M. Nofz, L. Wondraczek, J. Deubener, Bulk elastic properties, hardness and fatigue of calcium aluminosilicate glasses in the intermediate-silica range, J. Non-Cryst. Solids 434 (2016) 1–12.

[40] V.Y. Livshits, D.G. Tennison, G.O. Karapetyan, Elastic properties of nongradient glasses and glasses synthesized by ion-exchange diffusion at temperatures above and below the glass point, Sov. J. Glas. Phys. Chem. 8 (4) (1982) 422–428.

[41] B. Bridge, N.D. Patel, D.N. Waters, On the elastic constants and structure of the pure inorganic oxide glasses, Phys. Status Solidi A 77 (2) (1983) 655–668.

[42] M.M. Smedskjaer, R.E. Youngman, J.C. Mauro, Impact of ZnO on the structure and properties of sodium aluminosilicate glasses: comparison with alkaline earth oxides, J. Non-Cryst. Solids 381 (2013) 58–64.

[43] M. Taylor, G. Brown, Structure of mineral glasses.2. SiO_2–$NaAlSiO_4$ join, Geochim. Cosmochim. Acta 43 (9) (1979) 1467–1473.

[44] J. Murdoch, J. Stebbins, I. Carmichael, High-resolution Si-29 NMR-study of silcate and aluminosilicate glasses - the effect of network-modifying cations, Am. Mineral. 70 (3–4) (1985) 332–343.

[45] S.V. Nemilov, Viscous flow of glasses correlated with their structure. Application of the rate theory, Sov. J. Glas. Phys. Chem. 18 (1992) 1–27.

[46] W.H. Wang, Correlations between elastic moduli and properties in bulk metallic glasses, J. Appl. Phys. 99 (9) (2006) 093506.